The density dependence of the velocity of sound in expanded liquid mercury studied by means of a large-scale molecular-dynamics simulation

1998 J. Phys.: Condens. Matter 10 4963

(http://iopscience.iop.org/0953-8984/10/23/005)

J. Phys.: Condens. Matter **10** (1998) 4963–4974. Printed in the UK PII: S0953-8984(98)92658-3

The density dependence of the velocity of sound in expanded liquid mercury studied by means of a large-scale molecular-dynamics simulation

Shuji Munejiri, Fuyuki Shimojo and Kozo Hoshino

Faculty of Integrated Arts and Sciences, Hiroshima University, Higashi-Hiroshima 739-8521, Japan

Received 20 March 1998, in final form 28 April 1998

Abstract. The density dependence of the velocity of sound in liquid mercury along the liquid–vapour coexistence curve is investigated by means of a large-scale molecular-dynamics simulation using the effective pair potential derived from the experimental structure factor by the inverse method. The resulting velocity of sound is in very good agreement with experiment and its density dependence changes at 9 g cm^{-3}, at which point the metal–nonmetal transition occurs. It is shown that the repulsive part of the effective pair potential plays a crucially important role in the density dependence of the velocity of sound in liquid mercury.

1. Introduction

The velocities of sound in fluid mercury have been measured over a wide range of density from the triple point to the supercritical region. It was discovered for the first time by Suzuki *et al* [1] that the density dependence of the velocity of sound in liquid mercury changes at the density 9 g cm^{-3}, at which point the metal–nonmetal (M–NM) transition occurs. With density decreasing from the triple point, the velocity of sound decreases linearly until the M–NM transition region is neared, whereas its rate of decrease becomes smaller over that region until the critical region is neared. This feature has been confirmed by several successive experiments [2–4]. The change of the density dependence of the velocity of sound at the M–NM transition has been considered to be closely related to a change in the interaction between atoms [1], though the relation between the interatomic interaction and the velocity of sound is not well understood theoretically.

Recently, Nagel *et al* [5] calculated the structure factors of expanded liquid mercury for a wide range of density using the effective pair potentials obtained from pseudopotential perturbation theory for a metallic liquid and the Lennard-Jones potential for an insulating vapour. They compared their results with experiments and concluded that further details of the variation of the interatomic correlations with the density have to be included to reproduce the experimental structure factors for a wide range of density. Though these pair potentials are valid in the two corresponding limiting cases, they lose their validity for those states that are near the M–NM transition. At present, there is no method of deriving the effective pair potential for those states from first-principles theory.

In this situation, one of the most effective approaches is the inverse method, in which the effective pair potential is derived from the experimental structure factor. Recently, we have derived the effective pair potentials for expanded liquid rubidium and caesium for a

0953-8984/98/234963+12$19.50

wide range of density using the predictor–corrector method [6], which is one of the most reliable methods for solving the inverse problem, and investigated the characteristic features of their density dependences [7–9]. The purposes of this paper are as follows:

(i) to derive the effective pair potential from the experimental structural data for liquid mercury for a wide range of density [10] using the inverse method and to investigate their density dependences;

(ii) to calculate the velocity of sound by means of molecular-dynamics (MD) simulation using the effective pair potentials thus obtained;

(iii) to clarify the relation between the density dependence of the velocity of sound and that of the effective pair potential.

2. The method of calculation

2.1. The effective pair potential

In this section, the predictor–corrector method for solving the inverse problem is explained; it is a combination of integral equation theory and computer simulation. In the integral equation theory, the effective pair potential $\phi(r)$ is given by the following closure relation:

$$\beta\phi(r) = g_{\exp}(r) - 1 - c_{\exp}(r) - \ln g_{\exp}(r) + B_{\exp}(r) \tag{1}$$

where $g_{\exp}(r)$ is the experimental radial distribution function, $c_{\exp}(r)$ the experimental direct correlation function, $B_{\exp}(r)$ the experimental bridge function and $\beta = 1/k_{\mathrm{B}}T$. The functions $g_{\exp}(r)$ and $c_{\exp}(r)$ can be directly obtained from the experimental structure factor $S_{\exp}(k)$ by Fourier transformation and from the Ornstein–Zernike relation, respectively:

$$g_{\exp}(r) = 1 + \frac{1}{2\pi^2 nr}\int_0^\infty (S_{\exp}(k) - 1)k\sin(kr)\ \mathrm{d}k \tag{2}$$

$$c_{\exp}(r) = \frac{1}{2\pi^2 nr}\int_0^\infty \left(1 - \frac{1}{S_{\exp}(k)}\right)k\sin(kr)\ \mathrm{d}k \tag{3}$$

where n is the number density of the atoms. Though the key quantity in equation (1) is $B_{\exp}(r)$, it cannot be obtained directly from $S_{\exp}(k)$. To overcome this difficulty, we employ the bridge function of the hard-sphere system $B_{\mathrm{HS}}(r, \eta)$ as an initial estimate for $B_{\exp}(r)$, where the packing fraction η is determined so as to minimize the free energy [11] as is usually done in the modified hypernetted-chain (MHNC) approximation [12]. Thus the zeroth approximation for the effective pair potential is given by

$$\beta\phi_0(r) = g_{\exp}(r) - 1 - c_{\exp}(r) - \ln g_{\exp}(r) + B_{\mathrm{HS}}(r, \eta). \tag{4}$$

This approximation is called the predictor, and then $\phi_0(r)$ or $B_{\mathrm{HS}}(r, \eta)$ is improved by the following iterative procedure, which is called the corrector.

(i) The simulation is performed with $\phi_i(r)$ ($=\phi_0(r)$ for the first run) and the radial distribution function $g_i(r)$ is obtained, where i stands for the ith step.

(ii) The structure factor $S_i(k)$ is obtained by Fourier transforming $g_i(r)$.

(iii) The direct correlation function $c_i(r)$ is obtained using equation (3), where the subscript 'exp' is replaced by i.

(iv) The revised bridge function $B_i(r)$ is given by

$$B_i(r) = \beta\phi_i(r) - g_i(r) + 1 + c_i(r) + \ln g_i(r). \tag{5}$$

(v) The revised effective pair potential $\phi_{i+1}(r)$ is then given by

$$\beta\phi_{i+1}(r) = g_{\exp}(r) - 1 - c_{\exp}(r) - \ln g_{\exp}(r) + B_i(r). \tag{6}$$

The iterative process (i)–(v) is repeated until the difference $|\phi_{i+1}(r)-\phi_i(r)|$ becomes smaller than the desired accuracy and an accurate estimate for $\phi(r)$ is finally obtained. In this paper we are concerned with liquid mercury at relatively high temperatures and low densities, where the bridge function is expected to be small. If the contribution to the effective pair potential from the bridge function is not important, not only the first estimate for $\phi(r)$, where $B_{\mathrm{HS}}(r,\eta)$ is employed, but also the hypernetted-chain approximation, where the bridge function is taken to be zero, are considered to be reasonable approximations for the effective pair potential. This is the case, as will be shown in the following.

2.2. The dynamic structure factor and the velocity of sound

The velocity of sound is obtained by means of MD simulation as follows. First, the Fourier transform of the number density $n_{\boldsymbol{k}}(t)$ is calculated from the configuration of atoms at each MD step from

$$n_{\boldsymbol{k}}(t) = \sum_{i=1}^{N} \exp(-\mathrm{i}\boldsymbol{k}\cdot\boldsymbol{r}_i(t)) \tag{7}$$

where N is the total number of atoms. The intermediate scattering function is given by

$$F(k,t) = \frac{1}{N}\langle n_{\boldsymbol{k}}(t) n_{-\boldsymbol{k}}(0)\rangle \tag{8}$$

where $\langle\cdots\rangle$ means the average over time steps. Note that $F(k,t)$ is an even function of time and that $S(k) = F(k,0)$. The dynamic structure factor $S(k,\omega)$ is given by the Fourier transform of $F(k,t)$:

$$S(k,\omega) = \frac{1}{2\pi}\int_{-\infty}^{\infty} F(k,t)\exp(-\mathrm{i}\omega t)\ \mathrm{d}t = \frac{1}{\pi}\int_{0}^{\infty} F(k,t)\cos(\omega t)\ \mathrm{d}t. \tag{9}$$

The dispersion relation of $S(k,\omega)$ is obtained from the position of the side peak $\omega_{\mathrm{p}}(k)$ of $S(k,\omega)$. In the small-k region, $\omega_{\mathrm{p}}(k)$ satisfies the following relation:

$$\omega_{\mathrm{p}}(k) = v_{\mathrm{s}}k \tag{10}$$

where v_{s} is the velocity of sound. Thus v_{s} can be obtained from the gradient of the dispersion curve in the small-k region.

To derive the dispersion relation of $S(k,\omega)$, we need to obtain the $S(k,\omega)$ which has a clear side peak. In general, the side peak of $S(k,\omega)$ is clearly seen for small k and it becomes less clear with increasing k. Near the triple point there exists a clear side peak of $S(k,\omega)$ even for the relatively large k near the first peak position of $S(k)$. The side peak for such a large-k region, however, disappears with decreasing density and increasing temperature, and the clear side peak appears only in the very-small-k region. Therefore, when the density is low and the temperature is high, the size of the MD cell L must be large enough, i.e. $k_{\min} = 2\pi/L$ must be small enough, for the dynamic structure factor to have a side peak, from which we can obtain the velocity of sound. Furthermore, we have to continue the MD simulation for a very long time to obtain the spectrum of the correlation functions for a long wavelength, because the longer the wavelength is, the more slowly its density fluctuation decays. For these reasons, we perform in this paper a large-scale MD simulation using parallel computers to obtain the velocity of sound in liquid mercury.

As an alternative method for estimating the velocity of sound, the dispersion relation of the spectrum of the longitudinal current correlation function $J_l(k,\omega)$ is often used. $J_l(k,\omega)$ is related to the dynamic structure factor $S(k,\omega)$ as follows:

$$J_l(k,\omega) = \frac{\omega^2}{k^2} S(k,\omega). \tag{11}$$

Unlike $S(k,\omega)$, $J_l(k,\omega)$ always has a dispersion peak over the whole k-region. When $S(k,\omega)$ has a sharp side peak, the position of the peak of $J_l(k,\omega)$, $\omega_{max}(k)$, is almost the same as $\omega_p(k)$ and hence v_s obtained from $J_l(k,\omega)$ is the same as that obtained from $S(k,\omega)$. On the other hand, when the side peak of $S(k,\omega)$ is broad or does not exist, v_s obtained from $\omega_{max}(k)$ is larger than the real velocity of sound. Therefore we have to calculate v_s from $\omega_p(k)$ to get an accurate velocity of sound.

In addition to those quantities that we have just mentioned above, we also investigate the density dependence of the self-diffusion coefficient D, which is calculated from the relation

$$D = \frac{1}{3}\int_0^\infty Z(t)\ \mathrm{d}t \tag{12}$$

where $Z(t)$ is the velocity autocorrelation function defined by

$$Z(t) = \frac{1}{N}\sum_{i=1}^{N}\langle \boldsymbol{v}_i(t)\cdot\boldsymbol{v}_i(0)\rangle. \tag{13}$$

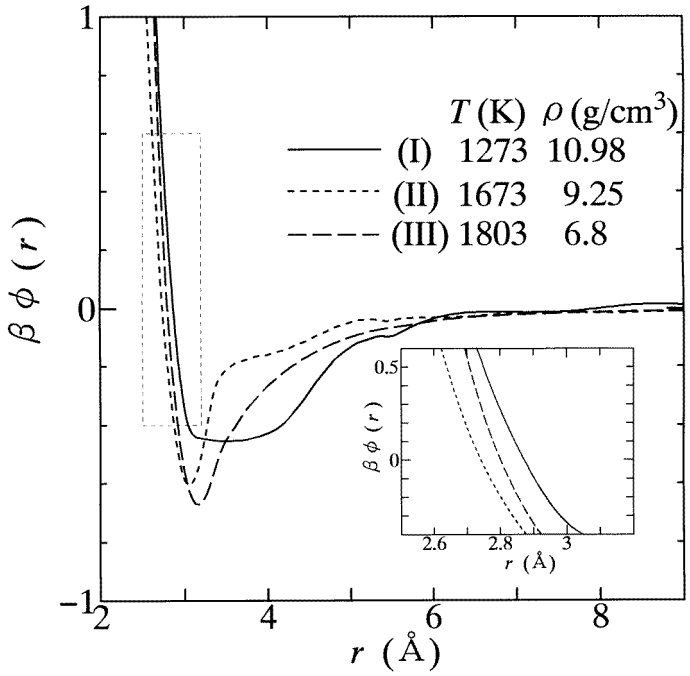

Figure 1. The effective pair potentials $\phi(r)$ for liquid mercury for the three states obtained by the inverse method. The inset shows an enlarged view of the repulsive part of $\phi(r)$.

Table 1. The parameters used in our MD simulation for three thermodynamic states.

State	T (K)	ρ (g cm^{-3})	n (Å^{-3})	N	L (Å)	$k_{\min}$ (Å^{-1})
I	1273	10.98	0.032 964	8000	62.4	0.101
II	1673	9.25	0.027 770	8000	66.0	0.095
				64 000	132.1	0.048
III	1803	6.8	0.020 415	8000	73.2	0.086
				64 000	146.4	0.043

3. Results and discussion

3.1. The effective pair potential of expanded liquid mercury

The structure factors of fluid mercury, $S(k)$, were measured by Tamura and Hosokawa [10] using x-ray scattering for fifteen different thermodynamic states from the triple point up to the supercritical region along the liquid–vapour coexistence curve. To investigate the density dependence of the effective pair potentials, we choose three thermodynamic states: (I) the metallic state (1273 K, 10.98 g cm^{-3}), (II) the state near the M–NM transition (1673 K, 9.25 g cm^{-3}) and (III) the non-metallic state (1803 K, 6.8 g cm^{-3}). The effective pair potentials $\phi(r)$ are derived by the predictor–corrector method as mentioned in the previous section. Since the bridge functions are small for these three states, $\phi(r)$ is almost the same as its zeroth approximation $\phi_0(r)$ within the experimental error. The three forms of $\phi(r)$ for

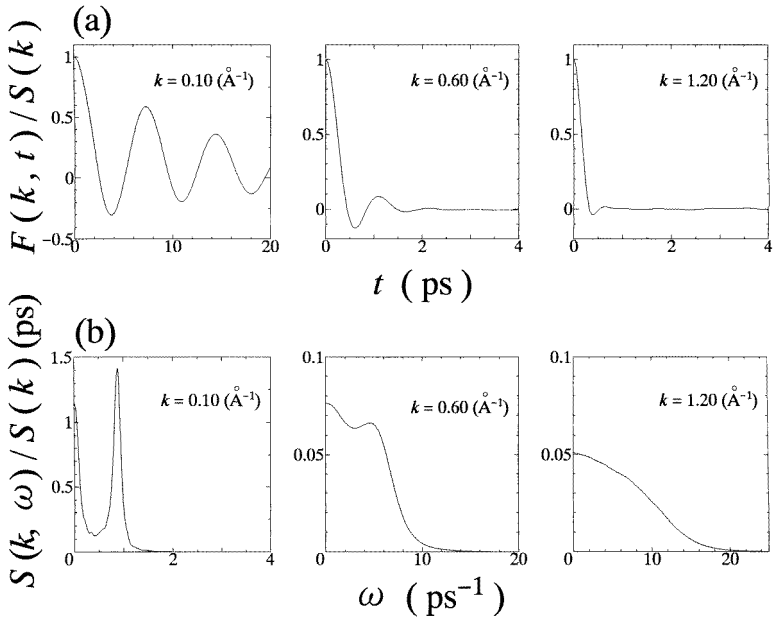

Figure 2. (a) Normalized intermediate scattering functions $F(k,t)/S(k)$ for $k = k_{\min} = 0.10, 0.60$ and 1.20 Å^{-1} for the state I (1273 K, 10.98 g cm^{-3}) obtained by means of MD simulation with 8000 atoms. (b) The corresponding dynamic structure factors $S(k,\omega)/S(k)$.

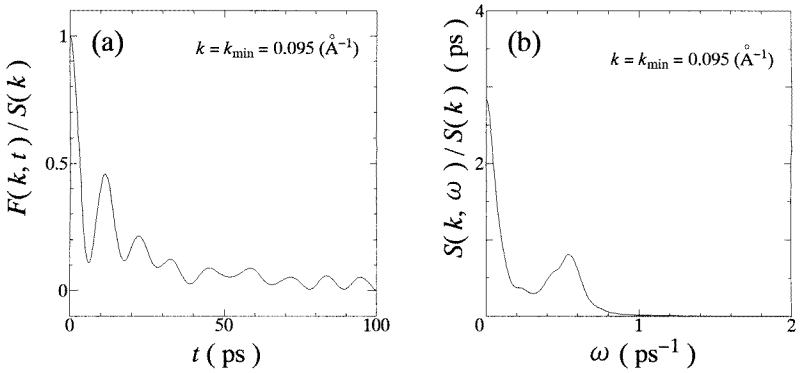

Figure 3. (a) Normalized intermediate scattering functions $F(k, t)/S(k)$ and (b) the dynamic structure factors $S(k, \omega)/S(k)$ for the state II (1673 K, 9.25 g cm^{-3}) for $k = k_{min}$. These results were obtained by means of MD simulation with a system of 8000 atoms.

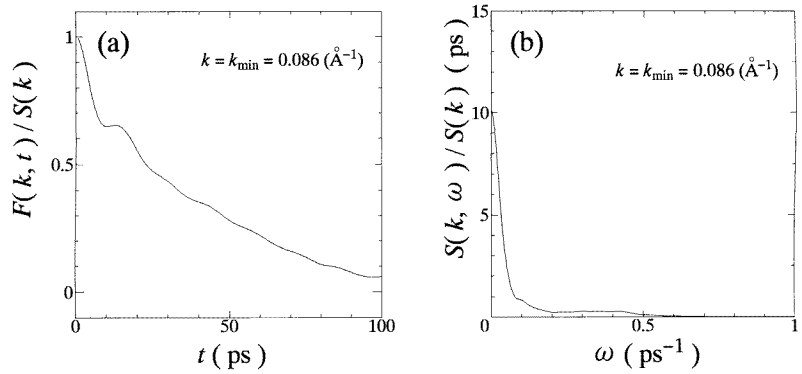

Figure 4. (a) Normalized intermediate scattering functions $F(k, t)/S(k)$ and (b) the dynamic structure factors $S(k, \omega)/S(k)$ for the state III (1803 K, 6.8 g cm^{-3}) for $k = k_{min}$. These results were obtained by means of MD simulation with a system of 8000 atoms.

liquid mercury thus obtained are shown in figure 1. The inset shows the enlarged repulsive part of $\phi(r)$. The characteristic features of $\phi(r)$ are as follows.

(i) The attractive well of $\phi(r)$ for a metallic state is broader than those for a nonmetallic state.

(ii) For state III, our $\phi(r)$ is very similar to the Lennard-Jones 6–12 potential used by Nagel *et al* [5]. However, we do not go into details of the density dependence of the attractive part of $\phi(r)$ for the following reason: since the structure of liquids is mainly determined by the repulsive part of the pair potential and the attractive part has only a small effect on the structure, it is not easy to derive the attractive part of $\phi(r)$ accurately from the experimental structure factor.

(iii) The repulsive part of $\phi(r)$ for the liquid mercury is harder than those for liquid rubidium and caesium.

(iv) When the state changes from I to II, the repulsive part of $\phi(r)$ shifts to a shorter distance. On the other hand, the repulsive part of $\phi(r)$ shifts to a longer distance again when the state changes from II to III.

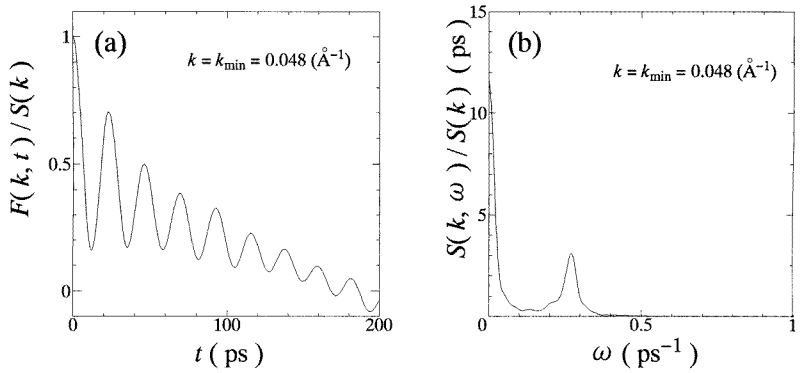

Figure 5. (a) Normalized intermediate scattering functions $F(k,t)/S(k)$ and (b) the dynamic structure factors $S(k,\omega)/S(k)$ for the state II (1673 K, 9.25 g cm^{-3}) for $k = k_{\min}$. These results were obtained by means of large-scale MD simulation with a system of 64 000 atoms.

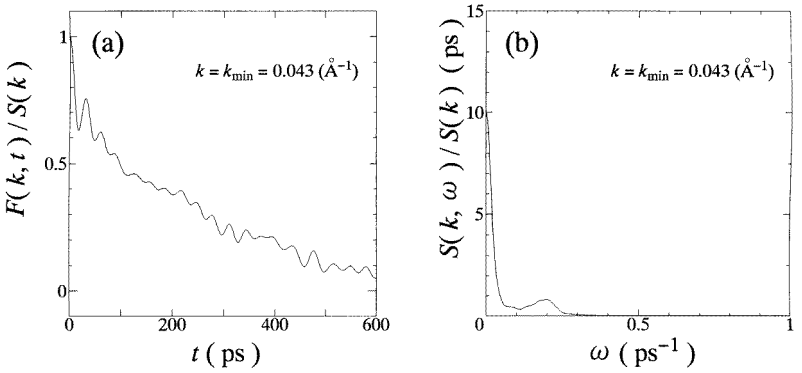

Figure 6. (a) Normalized intermediate scattering functions $F(k,t)/S(k)$ and (b) the dynamic structure factors $S(k,\omega)/S(k)$ for the state III (1803 K, 6.8 g cm^{-3}) for $k = k_{\min}$. These results were obtained by means of large-scale MD simulation with a system of 64 000 atoms.

3.2. The dynamic structure factor

To calculate the dynamic structure factor we perform the MD simulation using the effective pair potential obtained by the inverse method. A cubic MD cell with periodic boundary conditions is used. First, we carry out the MD simulation with 8000 atoms. The length of the side of the MD cell L is 62.4, 66.0 and 73.2 Å and the corresponding minimum wavenumber $k_{\min} = 2\pi/L$ is 0.101, 0.095 and 0.086 Å^{-1} for the states I, II and III, respectively. The parameters used in our MD simulation for these three states are shown in table 1.

Constant-temperature MD simulation [13] is employed. The cut-off distance of the effective pair potential is 12.0 Å. The time step is 4.8×10^{-15} s and the physical quantities are obtained by averaging over 200 000 time steps after the equilibrium state is reached. The normalized intermediate scattering functions $F(k,t)/S(k)$ for the three k-values for the state I and corresponding dynamic structure factors $S(k,\omega)/S(k)$ are shown in figure 2. $F(k,t)$ for small k, e.g. $k = 0.1$ Å^{-1}, clearly oscillates with the slow decay. With increasing k, the amplitude of the oscillation of $F(k,t)$ becomes smaller. As a result, though the side peak of $S(k,\omega)$ is well defined for a small k, it becomes to be less clear for large k.

$F(k,t)/S(k)$ and $S(k,\omega)/S(k)$ for the states II and III for $k = k_{\min}$ are shown in figures 3 and 4, respectively. With decreasing density and increasing temperature, the oscillation of $F(k,t)$ becomes vague and hence the side peak of $S(k,\omega)$ becomes broader even for $k_{\min}$. For the state III, the side peak cannot be recognized any longer even for $k_{\min}$, when the MD simulation is carried out for a system with 8000 atoms. To obtain the velocity of sound from the dispersion relation at low density and high temperature, we have to calculate $S(k,\omega)$ for a smaller k. Therefore we perform the MD simulation for a larger system consisting of 64 000 atoms for the states II and III. The side L of the cubic MD cell is 132.1 and 146.4 Å for the states II and III, respectively; these values are twice those for the system with 8000 atoms. Figures 5 and 6 show $F(k,t)/S(k)$ and $S(k,\omega)/S(k)$ for the state II and those for the state III for $k_{\min}$ for the case of 64 000 atoms (see table 1), respectively. Comparing figures 5 and 6 with figures 3 and 4, we see that the side peak of $S(k,\omega)$ for the state II is sharper and, even for the state III, it can be seen clearly.

Since the correlation length becomes very long near the critical point, it may be comparable with or even exceed the size of the MD cell. Therefore it is necessary to check whether the structure of the liquid depends on the system size or not, in particular near the critical point. As long as we compared dynamic structure factors obtained at the same wavenumber k for the two system sizes with each other, a clear size dependence of the structure was not found for the thermodynamic states studied here.

3.3. The velocity of sound and the effective pair potential

The dispersion relations $\omega_{\max}(k)$ obtained from the longitudinal current correlation functions are shown in figure 7(a). These results were obtained by means of MD simulations with 8000 atoms, except for a k smaller than $k_{\min}$ corresponding to 8000 atoms. In the small-k region, $\omega_{\max}(k)$ becomes smaller with decreasing density, which means that the velocity of sound decreases with decreasing density. Corresponding to the state dependence of the peak of $S(k)$, the minimum in these dispersion curves becomes shallower and shifts to a smaller k with decreasing density.

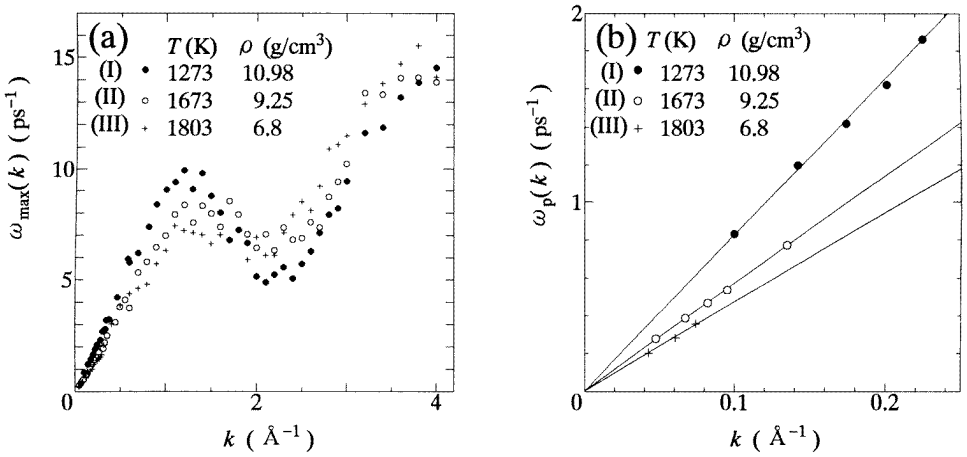

Figure 7. (a) Dispersion relations for the longitudinal current correlation function for the three states I, II and III. (b) Dispersion relations for the dynamic structure factor for the three states. The fitted lines for small k are also shown and their gradients correspond to velocities of sound.

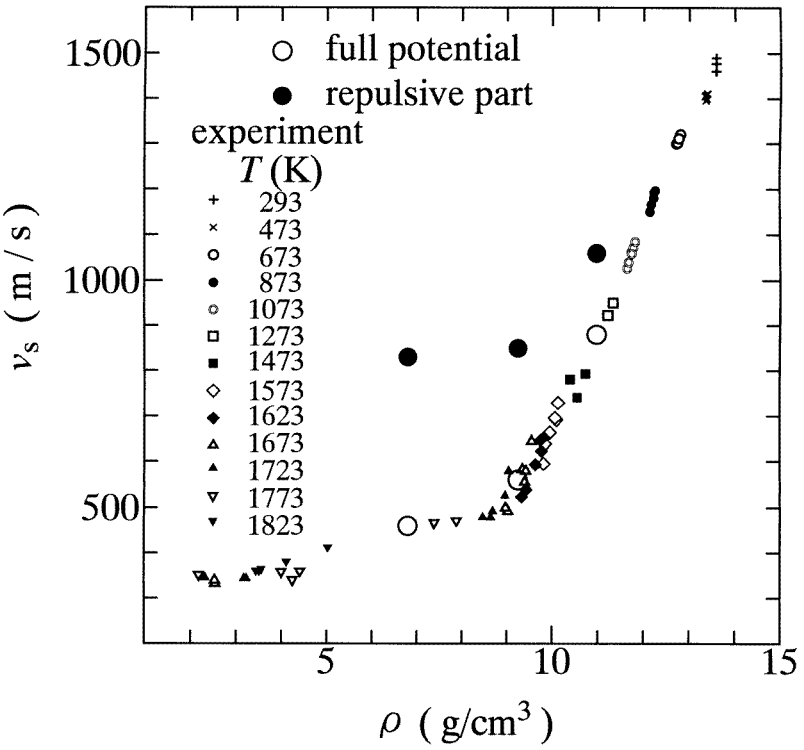

Figure 8. The density dependence of the velocity of sound v_s obtained by means of MD simulation (large open circles) and experimental data (the other, small symbols). The velocities of sound obtained using only the repulsive part of the effective pair potentials are also shown (large solid circles).

The dispersion relation $\omega_p(k)$ obtained from the side peak of the dynamic structure factors in the small-k region is shown in figure 7(b). Note that these dispersion relations cannot be obtained beyond the wavenumbers for which the side peaks of $S(k, \omega)$ can still be recognized. The results are well fitted by the straight lines. The values of v_s obtained from the gradients of these lines are compared with the experimental data [4] in figure 8. It is found that the calculated velocities of sound are in very good agreement with the experiments and that the characteristic features of the density dependence of the velocity of sound are well reproduced.

To investigate which parts of the effective pair potentials play an important role in the density dependence of the velocity of sound, we performed MD simulations using only the repulsive part of $\phi(r)$ and obtained the corresponding sound velocities. The results are shown by the big solid circles in figure 8. We find that, comparing with the density dependence of the velocity of sound obtained with the full potential, the results obtained using only the repulsive part of $\phi(r)$ show the characteristic features clearly at the M–NM transition. The attractive part of $\phi(r)$ tends to reduce the velocity of sound and this effect increases with decreasing density. Furthermore, the attractive parts make the inflection of the velocities of sound at 9 g cm^{-3} weak. We conclude from these results that the density dependence of the repulsive part of $\phi(r)$ plays a crucially important role in the velocity of sound having the inflection of its density dependence at the M–NM transition.

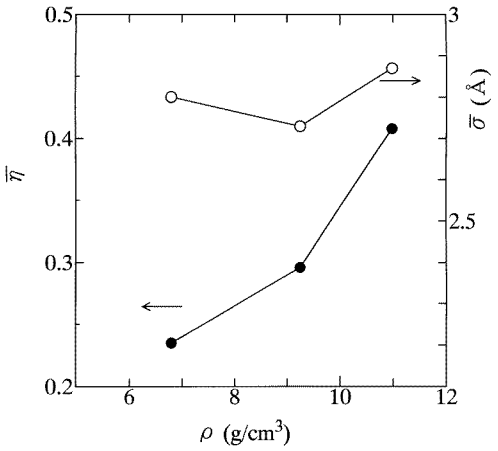

Figure 9. Density variations of the effective packing fraction $\bar{\eta}$ and the effective diameter $\bar{\sigma}$.

To clarify the density dependence of the repulsive part of $\phi(r)$ quantitatively, we define 'the effective diameter' $\bar{\sigma}$ by $\phi(\bar{\sigma}) = 0$ in the repulsive core region and 'the effective packing fraction' $\bar{\eta}$ as

$$\bar{\eta} = \frac{N(4\pi/3)(\bar{\sigma}/2)^3}{V} = \frac{n\pi\bar{\sigma}^3}{6} \tag{14}$$

where V is the volume of the system. The density variations of $\bar{\sigma}$ and $\bar{\eta}$ are shown in figure 9. With decreasing density, $\bar{\sigma}$ becomes smaller at first and then becomes larger after the M–NM transition occurs. It should be noted that a similar density dependence of the hard-sphere diameter was found by Götzlaff [14], who analysed the thermodynamic properties of liquid mercury on the basis of the hard-sphere model.

As a result of this behaviour of $\bar{\sigma}$, the density dependence of $\bar{\eta}$ changes at the M–NM transition in a similar way to the velocities of sound. It is considered that, in general, the velocity of sound is faster in a system with a higher packing fraction than in a system with a lower packing fraction. This is why the velocity of sound shows the steep decrease up to near the M–NM transition region and why its rate of decrease becomes smaller over that region until the critical region is neared.

The velocity of sound in liquid argon slows down linearly with decreasing density up to near the critical point and its gradient with respect to the density lies between those of the metallic state and the nonmetallic state of liquid mercury [1]. As for the gradient of the velocities of sound, the exponent $\log v_s / \log \rho$ at constant temperature was estimated by Okada and co-workers [4]. They found that the exponent for liquid mercury in the metallic state is 4 or 5, while it is 3 for argon. If the effective pair potential does not depend on the density, as in the case of liquid argon, the gradient of the velocity of sound with respect to the density would be the mean of the values for the metallic states and the nonmetallic states of liquid mercury. To confirm this, we performed a MD simulation for the three states I, II and III using $\phi(r)$ obtained for state III (6.8 g cm^{-3} and 1803 K) and calculated the velocities of sound. We found that the velocity of sound thus obtained does not bend but decreases almost linearly with decreasing density and its gradient with respect to the density certainly takes a value intermediate between those of the metallic and nonmetallic states.

Though there are no experimental data available for the self-diffusion coefficient D of liquid mercury, we calculated it from equation (12) for the three thermodynamic states and

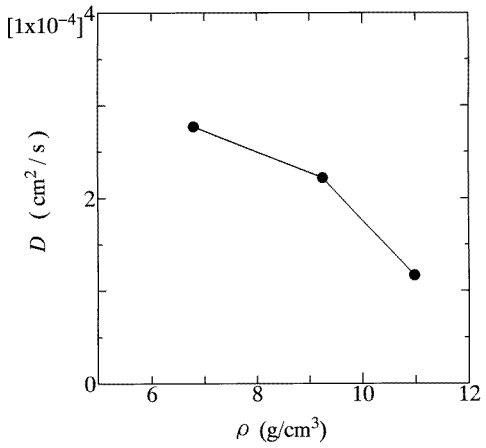

Figure 10. The density dependence of the self-diffusion coefficient D calculated from the velocity autocorrelation function obtained by means of MD simulation.

show our results in figure 10. It is seen from this figure that the density dependence of D changes at the M–NM transition, reflecting the variation of the packing fraction $\bar{\eta}$.

In a metallic state the effective pair potential is determined by the ion–ion direct Coulomb interaction and the indirect interaction due to the screening effect of conduction electrons. With decreasing density, the screening effect becomes weaker. In fact, it is well known that, with decreasing density or decreasing screening effect, the parameter $\bar{\sigma}$ of the effective pair potential of liquid alkali metals obtained from the pseudopotential perturbation theory becomes smaller. In addition to this decline of the screening effect, we should consider the fluctuation of the ionic structure near the M–NM transition point. Since density fluctuations increase with decreasing density, the valence electrons tend to localize rather than spread over a whole system like a uniform electron gas. This electron localization can be a reason for the repulsive part shifting towards a shorter distance with decreasing density in the metallic states. On the other hand, at lower densities than that at which the M–NM transition occurs, the liquid tends to change, with decreasing density, from a mixture of ions and valence electrons to one of neutral atoms and clusters. Since the diameter of a neutral atom is larger than that of an ion, the repulsive part of the effective pair potential shifts to a larger distance.

4. Summary

The density dependence of the velocity of sound in liquid mercury along the liquid–vapour coexistence curve is investigated by means of large-scale molecular-dynamics simulation with the effective pair potentials derived from the experimental static structure factors by the inverse method. The calculated velocities of sound are in very good agreement with experiments; the inflection of the density dependence of the velocity of sound is well reproduced. We have shown that the change in the density dependence of the velocity of sound at the M–NM transition can be explained by the change of the repulsive part of the effective pair potentials. We have also found that the density dependence of the self-diffusion coefficient changes at the M–NM transition for the same reason.

Acknowledgments

We are grateful to Professor K Tamura and Dr S Hosokawa for useful discussions and Dr K Okada and Professor M Yao for providing us with their experimental data. This work was supported by a Grant-in-Aid for Scientific Research on Priority Areas (No 07236102) from the Ministry of Education, Science, Sports and Culture. We thank the Japan Atomic Energy Research Institute (JAERI) for the use of the parallel supercomputer Fujitsu VPP300. We also acknowledge the Supercomputer Centre, Institute for Solid State Physics, University of Tokyo, for the use of the Fujitsu VPP500.

References

[1] Suzuki K, Inutake M, Fujiwaka S, Yao M and Endo H 1980 *J. Physique Coll.* **41** C8 66
[2] Kozhevnikov V F, Naurzakov S P and Arnold D I 1993 *J. Moscow Phys. Soc.* **3** 191
[3] Kozhevnikov V F, Naurzakov S P, Grodzinskii E and Arnold D I 1996 *J. Non-Cryst. Solids* **205–207** 256
[4] Yao M, Okada K, Aoki T and Endo H 1996 *J. Non-Cryst. Solids* **205–207** 274
Okada K, Odawara A and Yao M 1998 *Rev. High Pressure Sci. Technol.* **7** 736
[5] Nagel S, Redmer R and Röpke G 1996 *J. Non-Cryst. Solids* **205–207** 247
[6] Reatto L, Levesque D and Weis J J 1986 *Phys. Rev.* A **33** 3451
[7] Munejiri S, Shimojo F, Hoshino K and Watabe M 1995 *J. Phys. Soc. Japan.* **64** 344
[8] Munejiri S, Shimojo F, Hoshino K and Watabe M 1996 *J. Non-Cryst. Solids* **205–207** 278
[9] Munejiri S, Shimojo F, Hoshino K and Watabe M 1997 *J. Phys.: Condens. Matter* **9** 3303
[10] Tamura K and Hosokawa S 1994 *J. Phys.: Condens. Matter* **6** 419
[11] Lado F, Foiles S M and Ashcroft N W 1983 *Phys. Rev.* A **28** 2374
[12] Rosenfeld Y and Ashcroft N W 1979 *Phys. Rev.* A **20** 1208
[13] Nosé S 1984 *Mol. Phys.* **52** 255
[14] Götzlaff W 1988 *PhD Thesis* University of Marburg